Extension of MCC-FS model to bottom time-varying problems

B.B. Zhao[1], T.Y. Zhang[1], L.J. Li[1], Z. Wang[1,2,*], W.Y. Duan[1], M. Hayatdavoodi[1,3]

[1] College of Shipbuilding Engineering, Harbin Engineering University, Harbin, China

[2] Qingdao Innovation and Development Center of Harbin Engineering University, Qingdao, China

[3] School of Science and Engineering, University of Dundee, Dundee, UK

*zhan.wang@hrbeu.edu.cn

Highlights

- Equations of the Miyata-Choi-Camassa model that includes the free-surface effect (MCC-FS model) are extended to solve bottom time-varying problems.
- Waves generated by a moving obstacle on the bottom in a two-layer fluid system with a free surface is numerically simulated by use of the extended MCC-FS model.

1 Introduction

Internal wave is a common phenomenon in nature. Internal waves are generated by disturbances in the density stratified lakes and oceans. The model derived by Miyata (1985), Choi & Camassa (1999) (MCC, hereafter) is widely used to study large-amplitude internal waves in a two-layer fluid system. However, most of the studies on the MCC model are confined to the flat-bottom cases (Camassa et al., 2006; Jo & Choi, 2008; Kodaira et al., 2016; La Forgia & Sciortino, 2019; Zhao et al., 2020) or the cases where bottom only varied with space (Choi & Camassa, 1996; Choi et al., 2020).

For time-varying bottom in a two-layer fluid system, Grue et al. (1997) studied internal waves generated by a moving obstacle on the bottom by solving Euler's equations under the rigid-lid assumption (Euler-RL solution). Zhao et al. (2014) and Zhao & Duan (2014) used the two-layer high-level Green-Naghdi model to investigate the free-surface effect on the generated internal waves by comparing with Euler-RL solution of Grue et al. (1997).

In this paper, we will extend the MCC model that includes the free-surface effect (MCC-FS model) to solve bottom time-varying problems. This paper is organized as follows. The governing equations and boundary conditions of the extended MCC-FS model are described in Section 2. Numerical results of internal waves generated by a moving obstacle on the bottom in a two-layer fluid system with a free surface are presented and discussed in Section 3. Conclusions are reached in Section 4.

2 MCC-FS model

In this paper, we consider a two-layer fluid system with a free surface, shown in Figure 1. The two fluids are assumed to be inviscid, immiscible and incompressible. The origin of the Cartesian coordinate system is at the undisturbed interface between the two fluids. The mass densities of the upper and lower layers are ρ_1 and ρ_2, respectively. The undisturbed depths of the upper and lower layers are h_1 and h_2, respectively. The free surface, interface and bottom are expressed by $z = \eta_1(x, t)$, $z = \eta_2(x, t)$ and $z = \eta_3(x, t)$, respectively.

In the MCC-FS model, the governing equations include the mass conservation equations and the momentum conservation equations (Euler's equations), which in two dimensions can be written as

$$\frac{\partial u_i}{\partial x} + \frac{\partial w_i}{\partial z} = 0 \qquad (i = 1, 2), \tag{1}$$

$$\frac{\partial u_i}{\partial t} + u_i \frac{\partial u_i}{\partial x} + w_i \frac{\partial u_i}{\partial z} = -\frac{1}{\rho_i} \frac{\partial p_i}{\partial x} \qquad (i = 1, 2), \tag{2a}$$

$$\frac{\partial w_i}{\partial t} + u_i \frac{\partial w_i}{\partial x} + w_i \frac{\partial w_i}{\partial z} = -\frac{1}{\rho_i} \frac{\partial p_i}{\partial z} - g \qquad (i = 1, 2), \tag{2b}$$

where u and w are horizontal and vertical velocity components, respectively, p is the pressure and g is gravitational acceleration. $i = 1$ represents the variables for the upper-fluid layer and $i = 2$ represents the variables for the lower-fluid layer.

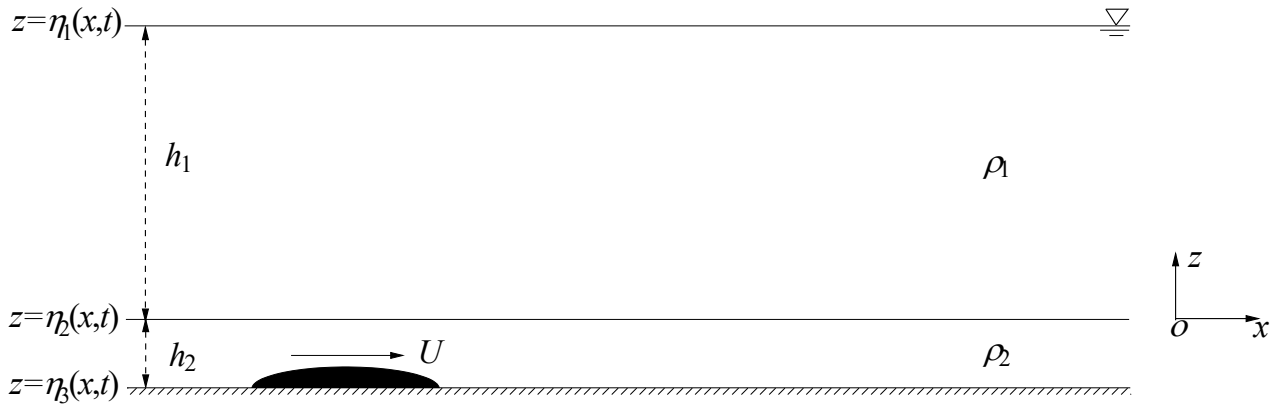

Figure 1 Sketch of a two-layer fluid system with a free surface

The boundary conditions for the upper-fluid layer are written as

$$w_1 = \frac{\partial \eta_1}{\partial t} + u_1 \frac{\partial \eta_1}{\partial x}, \quad \hat{p}_1 = 0 \quad \text{at } z = \eta_1(x,t), \tag{3a}$$

$$w_1 = \frac{\partial \eta_2}{\partial t} + u_1 \frac{\partial \eta_2}{\partial x} \quad \text{at } z = \eta_2(x,t), \tag{3b}$$

The boundary conditions for the lower-fluid layer are written as

$$w_2 = \frac{\partial \eta_2}{\partial t} + u_2 \frac{\partial \eta_2}{\partial x} \quad \text{at } z = \eta_2(x,t), \tag{4a}$$

$$w_2 = \frac{\partial \eta_3}{\partial t} + u_2 \frac{\partial \eta_3}{\partial x} \quad \text{at } z = \eta_3(x,t). \tag{4b}$$

The dynamic boundary condition at the interface between the two-fluid layers is written as

$$\overline{p}_1 = \hat{p}_2 \quad \text{at } z = \eta_2(x,t). \tag{5}$$

In the MCC-FS model, the depth-averaged horizontal velocity for each layer is defined as

$$\overline{u}_i(x,t) = \frac{1}{\eta_i - \eta_{i+1}} \int_{\eta_{i+1}}^{\eta_i} u_i(x,z,t)\mathrm{d}z \quad (i = 1,2). \tag{6}$$

The equations of the MCC-FS model for the flat bottom, i.e., $z = \eta_3(x, t) = -h_2$, can be written as (see e.g., Kodaira et al., 2016)

$$\frac{\partial \zeta_1}{\partial t} + \frac{\partial (\zeta_1 \overline{u}_1)}{\partial x} = 0, \quad \zeta_1 = \eta_1 - \eta_2, \tag{7a}$$

$$\frac{\partial \zeta_2}{\partial t} + \frac{\partial (\zeta_2 \overline{u}_2)}{\partial x} = 0, \quad \zeta_2 = \eta_2 - \eta_3, \tag{7b}$$

$$\frac{\partial \overline{u}_1}{\partial t} + \overline{u}_1 \frac{\partial \overline{u}_1}{\partial x} + g \frac{\partial}{\partial x}(\zeta_1 + \zeta_2) = \frac{1}{3\zeta_1} \frac{\partial}{\partial x}\left(\zeta_1^3 G_1\right) - \frac{1}{2\zeta_1} \frac{\partial}{\partial x}\left(\zeta_1^2 D_1^2 \zeta_2\right) + \frac{\partial \zeta_2}{\partial x}\left(\frac{1}{2}\zeta_1 G_1 - D_1^2 \zeta_2\right), \tag{7c}$$

$$\frac{\partial \overline{u}_2}{\partial t} + \overline{u}_2 \frac{\partial \overline{u}_2}{\partial x} + g \frac{\partial}{\partial x}\left(\frac{\rho_1}{\rho_2}\zeta_1 + \zeta_2\right) = \frac{1}{3\zeta_2} \frac{\partial}{\partial x}\left(\zeta_2^3 G_2\right) + \frac{\rho_1}{\rho_2} \frac{\partial}{\partial x}\left(\frac{1}{2}\zeta_1^2 G_1 - \zeta_1 D_1^2 \zeta_2\right), \tag{7d}$$

where

$$G_i(x,t) = \frac{\partial^2 \overline{u}_i}{\partial x \partial t} + \overline{u}_i \frac{\partial^2 \overline{u}_i}{\partial x^2} - \left(\frac{\partial \overline{u}_i}{\partial x}\right)^2, \quad D_i \equiv \frac{\partial}{\partial t} + \overline{u} \frac{\partial}{\partial x}. \tag{8}$$

In this paper, we extend the MCC-FS model to study the physical problem where the bottom varies with time and space, and hence Equations (7c) - (7d) are modified. The derivation process will be presented in the workshop.

3 Numerical results

Here, we numerically study the internal waves generated by a moving ellipse obstacle on the bottom in a two-layer fluid system with a free surface as shown in Figure 1. The parameters are the same as those given by Grue et al. (1997). Mass densities of the upper and lower layers are $\rho_1 = 787.3\mathrm{kg/m^3}$ and $\rho_2 = 1000\mathrm{kg/m^3}$, respectively. Undisturbed depths of the upper and lower layers are $h_1 = 0.12\mathrm{m}$ and $h_2 = 0.03\mathrm{m}$, respectively. The major-semi axis and the minor-semi axis of the moving ellipse obstacle are $L_{1/2} = 10h_2 = 0.3\mathrm{m}$ and $B_{1/2} = 0.1h_2 = 0.003\mathrm{m}$, respectively. The constant velocity of the obstacle is $U = 1.1c_0 = 0.252\mathrm{m/s}$, where $c_0 = [gh_1h_2(\rho_2-\rho_1)/(\rho_2h_1+\rho_1h_2)]^{1/2}$ is the linear long-wave speed. The initial

center position of the moving obstacle is at x = 0m.

We use the MCC-FS model to simulate the physical problem in time domain. We note that this case belongs to the shallow-configuration case (h_1/h_2 = 4/1) and the MCC-FS model can provide accurate results. Snapshots of the surface-wave elevation, internal-wave elevation and bottom at two different moments are shown in Figure 2.

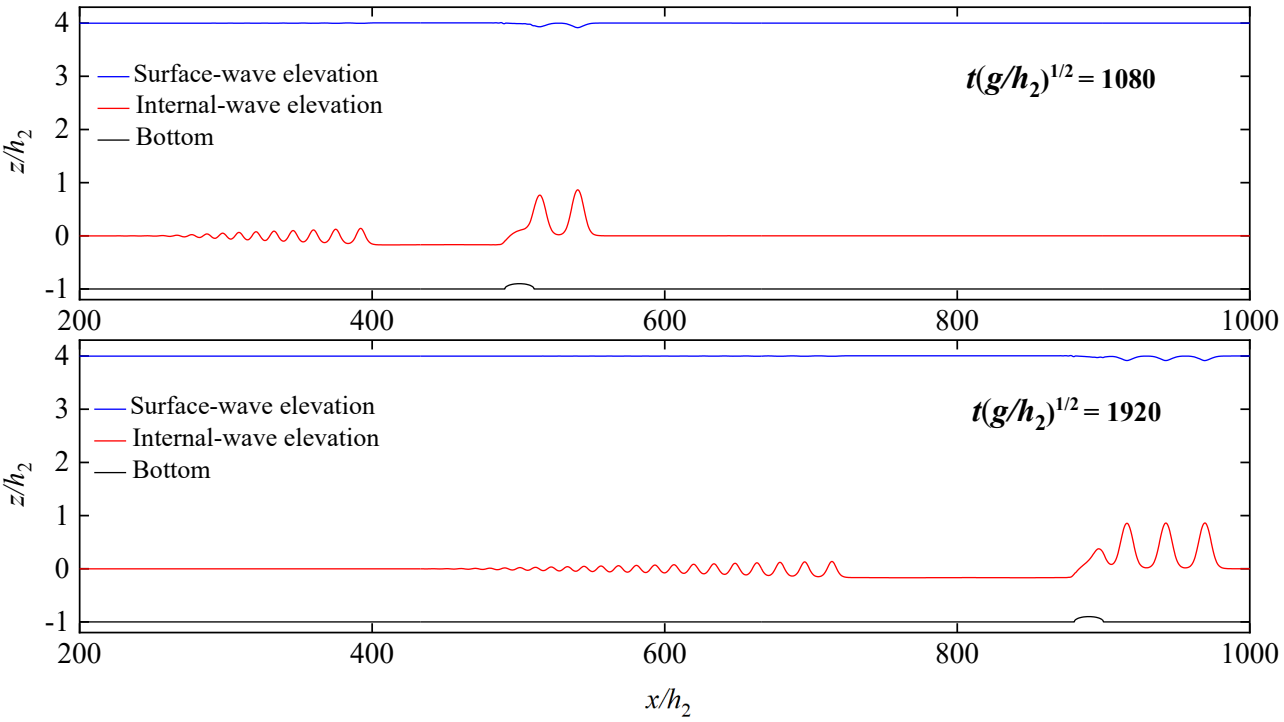

Figure 2 Snapshots of the elevations at different moments

As shown in Figure 2, surface waves in the depression form and internal waves in the elevation form are generated. With the time marching, the number of generated waves increases. At $t\,(g/h_2)^{1/2}$ = 1920, three complete surface waves with amplitude b/h_2 = –0.08 and three complete internal waves with amplitude a/h_2 = 0.86 are observed.

Next, we compare the internal-wave elevation results of the MCC-FS model with the results of the computational fluid dynamics (CFD) software, STAR-CCM+ and Euler-RL solution of Grue et al. (1997) and at $t\,(g/h_2)^{1/2}$ = 1920, as shown in Figure 3. We note that in the STAR-CCM+ simulations, the free-surface effect is included.

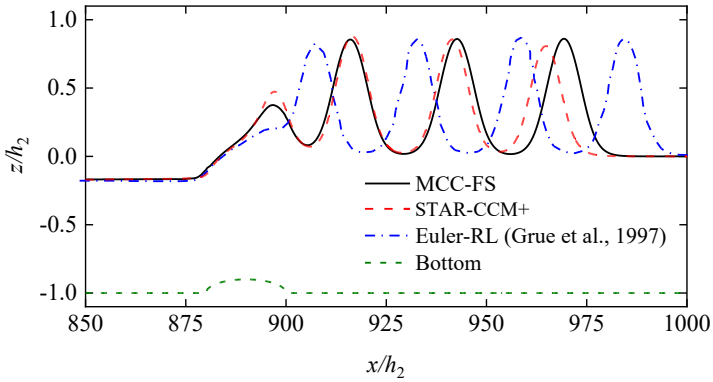

Figure 3 Comparison of internal-wave elevation obtained by the MCC-FS model, STAR-CCM+ and Euler-RL solution of Grue et al. (1997) at $t\,(g/h_2)^{1/2}$ = 1920

From Figure 3, we observe that four complete internal waves have been generated through the Euler-RL solution. While results of the MCC-FS model and STAR-CCM+ show that only three complete internal waves have been generated. Furthermore, the wave speed is smaller in the MCC-FS and STAR-CCM+ results compared with the Euler-RL solution. These differences are caused by the rigid-lid approximation introduced by Grue et al. (1997). Since the density ratio between the two fluids is not close to 1, the free-surface effect should be considered (Lamb, 1932), which is also observed in results shown in Figure 3.

The surface-wave elevation obtained by the MCC-FS model and STAR-CCM+ at $t\,(g/h_2)^{1/2}$ = 1920 is shown in Figure 4. We observe that three complete surface waves in the depression form have been generated. The amplitude of

the surface waves reaches $b/h_2 = -0.08$, which also implies that the free-surface effect should be included for this case where $\rho_1 / \rho_2 = 0.7873$.

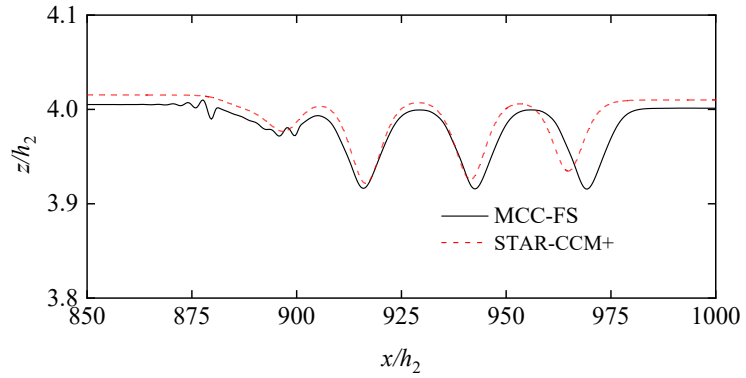

Figure 4 Surface-wave elevation obtained by the MCC-FS model and STAR-CCM+ at $t\,(g/h_2)^{1/2} = 1920$

4 Conclusions

In this paper, we extend the equations of the MCC-FS model to solve bottom time-varying problems. The internal waves generated by a moving obstacle on the bottom in a two-layer fluid system with a free surface is then numerically simulated. By comparing the MCC-FS results with the STAR-CCM+ results and the Euler-RL solution of Grue et al. (1997), we find that the number of generated waves is fewer and the wave speed is smaller when the free-surface effect is considered. Since the density ratio between the two fluids is not always close to 1, the rigid-lid approximation introduces larger errors in this case and the free-surface effect should be considered.

Acknowledgments

The first and fifth authors' (B.B. Zhao and W.Y. Duan) work is supported by the National Natural Science Foundation of China (No. 11972126) and the Heilongjiang Touyan Innovation Team Program.

References

[1] Miyata, M. (1985). An internal solitary wave with large amplitude. La Mar, 23: 43-48.
[2] Choi, W. & Camassa, R. (1999). Fully nonlinear internal waves in a two-fluid system. Journal of Fluid Mechanics, 396: 1-36.
[3] Camassa, R., Choi, W., Michallet, H., Rusas, P.-O. & Sveen, J.K. (2006). On the realm of validity of strongly nonlinear asymptotic approximations for internal waves. Journal of Fluid Mechanics, 549: 1-24.
[4] Jo, T.-C. & Choi, W. (2008). On Stabilizing the Strongly Nonlinear Internal Wave Model. Studies in Applied Mathematics, 120(1): 65-85.
[5] Kodaira, T., Waseda, T., Miyata, M. & Choi, W. (2016). Internal solitary waves in a two-fluid system with a free surface. Journal of Fluid Mechanics, 804: 201-223.
[6] La Forgia, G. & Sciortino, G. (2019). The role of the free surface on interfacial solitary waves. Physics of Fluids, 31: 106601.
[7] Zhao, B.B., Wang, Z., Duan, W.Y., Ertekin, R.C., Hayatdavoodi, M. & Zhang, T.Y. (2020). Experimental and numerical studies on internal solitary waves with a free surface. Journal of Fluid Mechanics, 899, A17.
[8] Choi, W. & Camassa, R. (1996). Weakly nonlinear internal waves in a two-fluid system. Journal of Fluid Mechanics, 313, 83-103.
[9] Choi, W., Zhi, C. & Barros, R. (2020). High-order unidirectional model with adjusted coefficients for large-amplitude long internal waves. Ocean Modelling, 151: 101643.
[10] Grue, J., Friis, H.A., Plam, E. & Rusas, P.O. (1997). A method for computing unsteady fully nonlinear interfacial waves. Journal of Fluid Mechanics, 351, 223-252.
[11] Zhao, B.B., Duan, W.Y., Ertekin, R.C. & Webster, W.C. (2014). Recent progress on the GN model for a two-layer flow. 29th International Workshop on Water Waves and Floating Bodies, Osaka, Japan.
[12] Zhao, B.B. & Duan, W.Y. (2014). Fluid-sheet water-wave theory—GN wave model. Tsinghua University Press (in Chinese).
[13] Lamb, H. (1932). Hydrodynamics, Dover.